

## Josephson supercurrent through a topological insulator surface state

M. Veldhorst,<sup>1</sup> M. Snelder,<sup>1</sup> M. Hoek,<sup>1</sup> T. Gang,<sup>1</sup> X.L. Wang,<sup>2</sup> V.K. Guduru,<sup>3</sup> U. Zeitler,<sup>3</sup> W.G. v.d. Wiel,<sup>1</sup> A.A. Golubov,<sup>1</sup> H. Hilgenkamp,<sup>1,\*</sup> and A. Brinkman<sup>1</sup>

<sup>1</sup>*Faculty of Science and Technology and MESA+ Institute for Nanotechnology,  
University of Twente, 7500 AE Enschede, The Netherlands*

<sup>2</sup>*Institute for Superconducting and Electronic Materials,  
University of Wollongong, Wollongong, NSW, 2522, Australia*

<sup>3</sup>*High Field Magnet Laboratory, Institute for Molecules and Materials,  
Radboud University Nijmegen, 6525 ED Nijmegen, The Netherlands*

(Dated: December 16, 2011)

Topological insulators [1–11] are characterized by an insulating bulk with a finite band gap and conducting edge or surface states, where charge carriers are protected against backscattering. These states give rise to the quantum spin Hall effect [2] without an external magnetic field, where electrons with opposite spins have opposite momentum at a given edge. The surface energy spectrum of a three-dimensional topological insulator [3, 5] is made up by an odd number of Dirac cones with the spin locked to the momentum. The long-sought yet elusive Majorana fermion [12] is predicted to arise from a combination of a superconductor and a topological insulator [13–15]. An essential step in the hunt for this emergent particle is the unequivocal observation of supercurrent in a topological phase. Here, we present the first measurement of a Josephson supercurrent through a topological insulator. Direct evidence for Josephson supercurrents in superconductor (Nb) - topological insulator ( $\text{Bi}_2\text{Te}_3$ ) - superconductor e-beam fabricated junctions is provided by the observation of clear Shapiro steps under microwave irradiation, and a Fraunhofer-type dependence of the critical current on magnetic field. The dependence of the critical current on temperature and length shows that the junctions are in the ballistic limit. Shubnikov-de Haas oscillations in magnetic fields up to 30 T reveal a topologically non-trivial two-dimensional surface state. We argue that the ballistic Josephson current is hosted by this surface state despite the fact that the normal state transport is dominated by diffusive bulk conductivity. The lateral Nb- $\text{Bi}_2\text{Te}_3$ -Nb junctions hence provide prospects for the realization of devices supporting Majorana fermions [16].

Almost simultaneous to the theoretical prediction of 3D topological insulator states in the bismuth compounds  $\text{Bi}_{1-x}\text{Sb}_x$ ,  $\text{Bi}_2\text{Se}_3$  and  $\text{Bi}_2\text{Te}_3$  [1], angle-resolved photoelectron spectroscopy indeed revealed a linear dispersion and a helical structure of the Dirac cone at the surface of these compounds [4, 7, 8]. Soon after, the topological nature of the surface states was confirmed by transport studies such as Aharonov-Bohm oscillations in  $\text{Bi}_2\text{Se}_3$  nanoribbons [9], Shubnikov-de-Haas oscillations in  $\text{Bi}_2\text{Te}_3$  [17–21], scanning tunneling spectroscopy of the square-root magnetic field dependence of the Landau level spacing [11] and interference effects resulting from impurity scattering [10]. Now the existence of the topological surface states has been established it is time to study the interaction with other materials. Efforts have been made to contact a topological insulator to a superconductor in the search for the Majorana fermion. First attempts [22, 23] indicated the presence of a supercurrent through a topological insulator, although no Josephson effects have been observed. In this Letter we demonstrate that it is possible to induce a Josephson supercurrent in the surface state of the topological insulator  $\text{Bi}_2\text{Te}_3$ , as evidenced by the two hallmarks of the Josephson effect: a Fraunhofer-like magnetic field modulation of the critical current and the

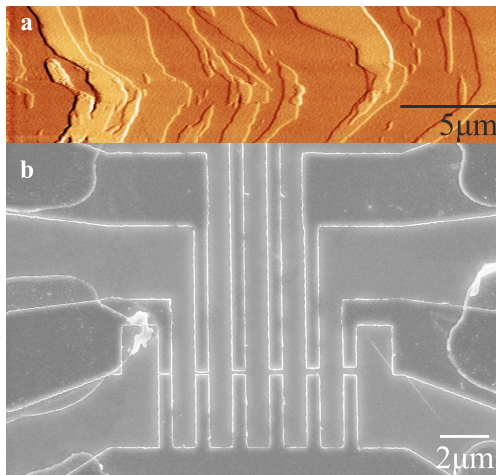


**FIG. 1: E-beam lithographically defined Nb electrodes on exfoliated  $\text{Bi}_2\text{Te}_3$ .** (a) Atomic force microscopy image of an exfoliated  $\text{Bi}_2\text{Te}_3$  surface. The step edges are 1.0 nm high, corresponding to the  $\text{Bi}_2\text{Te}_3$  quintuple unit cell. These nanometer flat surfaces span an area up to  $50 \times 50\ \mu\text{m}^2$ . (b) Scanning electron microscopy image of Nb- $\text{Bi}_2\text{Te}_3$ -Nb Josephson junctions. The Nb superconductor strips are defined by e-beam lithography on a 200 nm thick exfoliated  $\text{Bi}_2\text{Te}_3$  flake and connected to large Nb electrodes fabricated by photolithography. The junctions have a width of 500 nm and a length of (from left to right) 50, 100, 150, 200, 250 and 300 nm. A supercurrent has been identified at 1.6 K in all junctions up to 250 nm.

appearance of Shapiro steps upon microwave irradiation, resulting from the dc and ac Josephson effects, respectively.

We have fabricated polycrystalline  $\text{Bi}_2\text{Te}_3$  samples with a common  $c$ -axis orientation using the Czochralski method as described elsewhere [24]. From these, flakes were produced by mechanical cleaving, proven to be a powerful tool for the fabrication of a few quintuple layer thin  $\text{Bi}_2\text{Te}_3$  flakes [25]. Figure 1a shows an atomic force microscopy image of the surface of typical exfoliated  $\text{Bi}_2\text{Te}_3$  flakes. We have performed experiments on large flakes with atomically flat terraces, extending over several micrometers. The  $\text{Bi}_2\text{Te}_3$  quintuple layer step edges are clearly visible as shown in Fig. 1a. The exfoliated flakes have a thickness of  $20 \text{ nm} - 2 \mu\text{m}$ . Van der Waals forces bind the flakes to the Si-substrate, enabling subsequent sputtering of Nb electrodes by standard lift-off photolithography. E-beam lithography is used in a second step to define smaller Nb nanostructures by lift-off sputter deposition on top of the flake, connected to the larger Nb electrodes fabricated with photolithography. A scanning electron microscopy image of such a device is given in Fig. 1b.

To characterize the electronic properties of our devices and to track them down to the surface states of a topological insulator we have performed magnetotransport experiments on  $\text{Bi}_2\text{Te}_3$  flakes in a Van der Pauw geometry in fields up to 30 T. From the low field Hall coefficient  $R_H = 7.5 \times 10^{-8} \Omega\text{m/T}$  and the zero-field resistivity  $\rho = 300 \mu\Omega\text{cm}$  we deduce a bulk conductivity channel with an n-type carrier concentration  $n = 8.3 \times 10^{19} \text{ cm}^{-3}$  and mobility  $\mu = 250 \text{ cm}^2/\text{Vs}$  corresponding to an electron mean free path  $l_e = 22 \text{ nm}$  for a parabolic band. This low mobility would not allow the observation of quantum oscillations since the necessary condition,  $\mu B \gg 1$ , is far from being fulfilled in the magnetic fields applied. As shown in Fig. 2a, we nevertheless observe clear Shubnikov-de Haas oscillations in the resistance implying another conduction channel with larger mobility. From the angle dependence of the position of the peaks we conclude that this additional channel is of two-dimensional nature.

The oscillatory contribution to the resistance of such a two-dimensional system can be written as [26]

$$R_{xx} \propto \frac{\lambda}{\sinh \lambda} e^{-\lambda_D} \cos \left( \frac{2\pi E_F}{\hbar\omega_c} + \pi + \varphi_B \right) \quad (1)$$

where,  $\omega_c$  is the cyclotron frequency,  $E_F$  is the Fermi energy,  $\lambda = 2\pi^2 k_B T / \hbar\omega_c$ ,  $\lambda_D = 2\pi^2 k_B T_D / \hbar\omega_c$  with  $T_D$  the Dingle temperature, and  $\varphi_B$  is the Berry phase. When plotting the  $1/B$ -positions of the minima and maxima of  $R_{xx}$  (Fig. 2d) as a function of the Landau level index it already becomes clear that the corresponding  $1/B$ -positions do not extrapolate to  $\varphi_B = 0$  as one

would expect from an ordinary system, but is rather shifted by  $\frac{1}{2}$  implying that  $\varphi_B = \pi$ , consistent with a half-filled zeroth Landau level that is present in a topological surface state [17–21, 27], similar to graphene [28, 29]. From the slope in Fig. 2d we infer the carrier concentration of this surface state of  $n = 1.2 \times 10^{12} \text{ cm}^{-2}$ ; an effective mass  $m^* = 0.16 m_0$  and a Dingle temperature of  $T_D = 1.65 \text{ K}$  (corresponding to a mobility  $\mu = 8300 \text{ cm}^2/\text{Vs}$ ) follow from the temperature and field dependence of the Shubnikov-de Haas oscillations amplitudes (Figs. 2b and 2c). This results in a  $v_F = 1.4 \times 10^5 \text{ m/s}$  with  $l_e = 105 \text{ nm}$ .

In high magnetic fields two beating frequencies are present, as Xiong *et al.* [20] also observed in their study on the topological surface states of  $\text{Bi}_2\text{Te}_2\text{Se}$ . A double frequency has also been observed in the 3D topological insulator strained  $\text{HgTe}$  [27], where it was concluded to originate from the top and bottom topological surface states, with different carrier densities due to the difference in electrostatic environment (substrate and vacuum). As can be seen in Fig. 2a, the peak splitting becomes more pronounced with increasing parallel field, though it is already visible in the derivative of the magnetoresistance at smaller angles.

The superconducting  $\text{Nb-Bi}_2\text{Te}_3\text{-Nb}$  junctions, as depicted in Fig. 1b, show Shubnikov-de Haas oscillations at high magnetic fields with the same frequency, revealing the presence of topological surface states in these devices as well. The critical current of the Nb electrodes on top of the  $\text{Bi}_2\text{Te}_3$  is larger than 30 mA for a strip of 500 nm width and 70 nm height. The junctions have a metallic temperature dependence, but upon cooling below 6.5 K, the resistance vanishes completely and a supercurrent is observed. Figure 3a shows a current-voltage characteristic at 1.6 K showing a clear supercurrent of  $I_c = 18 \mu\text{A}$ . To test whether this is a true Josephson supercurrent we performed phase-sensitive experiments. Figure 3d shows the Fraunhofer pattern from the critical current dependence on the magnetic field due to the dc Josephson effect. The smaller sidelobes follow from the small ratio between the length and the width of the junction, as predicted by [30]. Due to the ac Josephson effect, microwave irradiation should lead to Shapiro steps. Figure 3a shows the  $IV$ -curve upon 10.0 GHz microwave irradiation. Clear steps are observed at integer values of  $V = h/2ef_{\text{RF}} = 20.7 \mu\text{V}$ . A colormap of the conductance dependence on the power and the current is shown in Fig. 3b, visualizing the evolution of the Shapiro steps. In Fig. 3c we have plotted the power dependence of the thirist three steps, following the expected Bessel function dependence.

Now that we have confirmed the Josephson nature of the devices, we can discuss in which band of the  $\text{Bi}_2\text{Te}_3$  the proximity effect is induced. Figure 4 shows the temperature and length dependence of the critical current of the junctions. While the scaling with length can be described

by diffusive as well as ballistic transport theory (see Suppl. Information for details), the temperature dependence of the junctions is clearly far from the diffusive limit and can only be fitted by the Eilenberger theory for ballistic junctions [31, 32]. The bulk mean free path,  $l_e = 22$  nm, is too small to explain the ballistic nature of the supercurrent in the junctions. However, the surface conduction band has a larger mean free path  $l_e = 105$  nm. Noting that the mean free path obtained from Shubnikov-de Haas oscillations is usually an underestimate [33], we conclude that the ballistic Josephson supercurrent is carried by the topological surface states of  $\text{Bi}_2\text{Te}_3$ . As we discuss in more detail in the Suppl. Information, the small  $I_c R_n$  product (reduced to about 2%) follows automatically from the large bulk shunt. The clean limit fit with  $T_c = 6.5$  K gives a coherence length  $\xi = \frac{\hbar v_F}{2\pi k_B T} = 75$  nm at 1.6 K, implying that  $v_F = 1.0 \times 10^5$  m/s. This Fermi velocity is comparable to the value obtained from the magnetoresistance oscillations of the surface states ( $1.4 \times 10^5$  m/s).

The possibility of contacting many electrodes on the exfoliated  $\text{Bi}_2\text{Te}_3$  flakes combined with the reproducibility as observed in the length dependence of the junctions creates an interesting basis for experimental investigations of the still increasing number of theoretical proposals on topological insulator - superconductor devices [13–15]. Interestingly, whereas bulk transport tends to obscure the observation of surface state transport in the normal state, the supercurrent is found to be carried mainly by the surface states. The realization of supercurrents through topological surface states is an important step towards the detection of Majorana fermions.

## Methods

By mechanical exfoliation on polycrystalline  $\text{Bi}_2\text{Te}_3$  samples, flakes of size up to  $50 \times 50 \mu\text{m}^2$  and thicknesses of 20 nm up to 2  $\mu\text{m}$  were transferred to Si substrates. Sputter deposited Nb(200nm)/Pd(5nm) electrodes were defined by lift off techniques using optical photolithography with image reversal photoresist. The Pd layer prevents the Nb from oxidation and the thickness of the Nb being on the order of the flake thickness ensures a superconducting contact ( $I_C > 30$  mA) between the Nb on the substrate and the flake. The Nb(70 nm) junctions were defined with lift off using e-beam and have a superconducting contact ( $I_C > 30$  mA) with the Nb electrodes. To obtain transparent contacts, the  $\text{Bi}_2\text{Te}_3$  surface is Ar sputter etched *in situ* prior to Nb deposition, while the  $\text{Bi}_2\text{Te}_3$  in between the Nb forming the actual junction is unaffected due to the lift off technique. The supercurrent is investigated in shielded cryostats with dedicated home build equipment and the angle dependent magnetoresistance is measured at the High Field Magnet Laboratory (Nijmegen) in a 33 T magnet.

## Acknowledgments

We acknowledge useful discussions with C.W.J. Beenakker, B.C. Kaas, M. Fuhrer, C.G. Moleenaar, L. Molenkamp, N. Nagaosa, Y.V. Nazarov and Y. Tanaka. This work is supported by the Netherlands Organization for Scientific Research (NWO) through VIDI and VICI grants, by the Dutch FOM foundation, and by the Australian Research Council through a Discovery project.

## - SUPPLEMENTARY INFORMATION -

### *Theoretical models for Josephson current*

Any hybrid structure containing superconductors can be described on the basis of the Gor'kov equations [34]. In practice, these equations are typically simplified by a quasi-classical approximation, which is justified as long as the Fermi-wavelength is much smaller than other length scales in the problem. For superconductor - normal metal - superconductor (SNS) Josephson junctions Eilenberger quasi-classical equations [35] are used when the elastic mean free path  $l_e$  is larger than the length  $L$  and the coherence length  $\xi$ . The electronic transport in this clean limit is ballistic across the N layer. In the dirty limit of  $l_e \ll L, \xi$ , transport is diffusive and the Usadel equations [36] are used. When the transparency between the S and N layers is not unity, additional insulating barriers (I) are typically included.

### *Eilenberger theory fit*

The clean limit theory on the basis of the Gor'kov equations for short SINIS junctions with arbitrary barrier transparency  $D$  [31] was generalized [32, 37] for arbitrary junction length on the basis of Eilenberger equations. The supercurrent density  $J$  is found to be [32]

$$J = \frac{2}{\pi} e k_F^2 k_B T \sin \chi \sum_{\omega_n > 0} \int_0^1 \mu d\mu \frac{t_1(\mu) t_2(\mu)}{Q^{1/2}(\chi, \mu)}, \quad (2)$$

where  $\mu = k_x/k_F$ ,  $t_{1,2} = D_{1,2}/(2 - D_{1,2})$ , and

$$Q = \left[ t_1 t_2 \cos \chi + \left( 1 + (t_1 t_2 + 1) \frac{\omega_n^2}{\Delta^2} \right) \cosh \frac{2\omega_n L}{\mu \hbar v_F} + (t_1 + t_2) \frac{\omega_n \Omega_n}{\Delta^2} \sinh \frac{2\omega_n L}{\mu \hbar v_F} \right]^2 - (1 - t_1^2) (1 - t_2^2) \frac{\Omega_n^4}{\Delta^4}, \quad (3)$$

where the Matsubara frequency is given by  $\omega_n = 2\pi k_B T (2n + 1)$ , and  $\Omega_n = \sqrt{\omega_n^2 + \Delta^2}$ .  $\Delta$  is the gap in the S electrodes,  $\chi$  the phase difference across the junction, while  $v_F$  is the Fermi velocity of the normal metal interlayer. The integral runs over all trajectory directions and can be adjusted to actual junction geometries.

Eq. (2) was evaluated as function of junction length and fitted to the measured critical current density. Since the prefactors in Eq. (2) implicitly contain the normal state resistance, which is not known for our junctions due to the bulk shunt, we left the overall scale of  $J$  free in the fit. Subsequently, the best fit to the data at 1.6 K was obtained for  $\xi = \frac{\hbar v_F}{2\pi k_B T} = 75$  nm. It was found numerically that the value of the barrier transparencies in the symmetric case had no influence on the fitting value for  $\xi$ .

The temperature dependence of the critical current was calculated using Eq. (2) and the obtained coherence length. The fit to the measured data is excellent, considering that only the overall scale of  $J$  was free in this case.

In fact, the overall scaling factor of the critical current in Eq. (1) can be estimated as well. The transparency of the interfaces between the topological insulator and the superconductor are important in this respect. The high transparency of our interfaces can be determined from the  $I(V)$  characteristic. The excess current in the  $I(V)$  characteristic is about 67% of the critical current  $I_c$ . In the Blonder-Tinkham-Klapwijk model [40], this gives a barrier strength of about  $Z = 0.6$ . For these high transparencies, at the lowest temperatures and for the 50 nm junction, Eq. (1) provides an  $I_c R_N$  product of the order of 1-2 mV. However the 3D bulk shunt will strongly reduce this value by decreasing  $R_n$ . From the Shubnikov de Haas oscillations we can estimate the surface to bulk resistance ratio. The surface resistance can be found through the amplitude of  $R_{SDH} = R_c \frac{\lambda}{\sinh \lambda} e^{-\lambda D}$ . With  $\frac{\lambda}{\sinh \lambda} e^{-\lambda D} = 0.77 \Omega$ , we estimate a surface resistance of about 2% of the total resistance. Thus, the estimated surface resistance is approximately 29  $\Omega$ , which together with  $I_c = 32 \mu\text{A}$  results in  $I_c R_N = 1$  mV, agreeing with the Eilenberger model. This quantitative agreement between model and measurements underlines the conclusion that supercurrent is flowing through the ballistic channels of the topological surfaces states, shunted by a normal state bulk conduction.

#### *Usadel theory fit*

The Usadel equation [36] for the S and N layers in a diffusive SNS junction can be written as

$$\Phi_{S,N} = \Delta_{S,N} + \xi_{S,N}^2 \frac{\pi k_B T_c}{\omega_n G_{S,N}} \frac{d}{dx} \left( G_{S,N}^2 \frac{d}{dx} \Phi_{S,N} \right), \quad (4)$$

where  $\Phi$  is defined in terms of the normal Green's function  $G$  and the anomalous Green's function  $F$  by  $\Phi G = \omega_n F$ . The normalization condition  $F F^* + G^2 = 1$  then gives

$$G_{S,N} = \frac{\omega_n}{\sqrt{\omega_n^2 + \Phi_{S,N} \Phi_{S,N}^*}} \quad (5)$$

The coherence length is given by  $\xi = \sqrt{\frac{\hbar D}{2\pi k_B T}}$  where  $D = v_F l_e / 3$  is the diffusion constant.

The pair potentials  $\Delta_{S,N}$  are given by

$$\Delta_{S,N} \ln \frac{T}{T_{cS,N}} + 2\pi k_B T \sum_{\omega_n > 0} \frac{\Delta_{S,N} - \Phi_{S,N} G_{S,N}}{\omega_n} = 0 \quad (6)$$

In the dirty limit, Zaitsev's effective boundary conditions for quasi-classical Green's functions were simplified by Kupriyanov and Lukichev [39]. When  $\Phi$  and  $G$  are found using these boundary conditions, finally the supercurrent density can be obtained from

$$J = \frac{2\pi k_B T}{e\rho_N} \text{Im} \sum_{\omega_n > 0} \frac{G_N^2}{\omega_n^2} \Phi_N \frac{d}{dx} \Phi_N, \quad (7)$$

where  $\rho_N$  is the N layer resistivity.

For junctions with arbitrary length and arbitrary barrier transparency, no analytical expressions exist for the Green's functions. Therefore a numerical code was used to fit the data. In the effective boundary conditions [39], two parameters play a role,  $\gamma = \frac{\rho_S \xi_S}{\rho_N \xi_N}$  and  $\gamma_B = \frac{2l_e}{3\xi_N} \langle \frac{1-D}{D} \rangle$ , where the average of the transparencies takes place over all trajectory angles. For Nb as S electrode and  $\text{Bi}_2\text{Te}_3$  as N interlayer,  $\gamma \ll 1$  because of the lower resistivity  $\rho$  of Nb as compared to  $\text{Bi}_2\text{Te}_3$ . The junctions transparency is not known a priori, but from the voltage drop over a barrier in the normal state, as well as the large amount of excess current (more than 50% of the critical current) in the current-voltage characteristics of the superconducting state, a conservative estimate gives  $D \gtrsim 0.5$ , which implies  $\gamma_B \lesssim 1$ . Within this parameter range (or even outside the range) no consistent fit could be made to the data. Figure 6a shows the fit to the temperature dependence of the critical current for  $\gamma = 0.1$ ,  $\gamma_B = 1$  and  $\xi(T_c) = \sqrt{\frac{\hbar D}{2\pi k_B T_c}} = 21$  nm, the latter value as obtained from fitting the length dependence of the junction.

---

\* Also at Leiden Institute of Physics, Leiden University, P.O. Box 9506, 2300 RA Leiden, The Netherlands

- [1] Bernevig, B.A. & Hughes, T.L. & Zhang, S.C. Quantum spin Hall effect and topological phase transition in HgTe quantum wells. *Science* **314**, 1757-1761 (2006).
- [2] König, M. *et al.* Quantum spin Hall insulator state in HgTe quantum wells. *Science* **318**, 766-770 (2007).
- [3] Fu, L. & Kane, C.L. & Mele, E.J. Topological insulators in three dimensions. *Phys. Rev. Lett.* **98**, 106803 (2007).



- [4] Hsieh, D. *et al.* A topological Dirac insulator in a quantum spin Hall phase. *Nature* **452**, 970-974 (2008).
- [5] Zhang, H. *et al.* Topological insulators  $\text{Bi}_2\text{Se}_3$ ,  $\text{Bi}_2\text{Te}_3$  and  $\text{Sb}_2\text{Te}_3$  with a single Dirac cone on the surface. *Nature Phys.* **5** 438-442 (2009).
- [6] Qi, X.L. & Rundong, L. & Zang, J. & Zhang, S.C. Inducing a magnetic monopole with topological surface states. *Science* **323**, 1184-1187 (2009).
- [7] Chen, Y.L. *et al.* Experimental realization of a three-dimensional topological insulator,  $\text{Bi}_2\text{Te}_3$ . *Science* **325**, 178-181 (2009).
- [8] Hsieh, D. *et al.* A tunable topological insulator in the spin helical Dirac transport regime. *Nature* **460**, 1101-1105 (2008).
- [9] Peng, H. *et al.* Aharonov-Bohm interference in topological insulator nanoribbons. *Nature Mat.* **9**, 225-229 (2010).
- [10] Zhang, T. *et al.* Experimental demonstration of topological surface states protected by time-reversal symmetry. *Phys. Rev. Lett.* **103**, 266803 (2009).
- [11] Cheng, P. *et al.* Landau quantization of topological surface states in  $\text{Bi}_2\text{Se}_3$ . *Phys. Rev. Lett.* **105** 076801 (2010).
- [12] Majorana, E. Teoria simmetrica dellelettrone e del positrone. *Nuovo Cimento* **14**, 171-184 (1937).
- [13] Fu, L. & Kane, C.L. & Mele, E.J. Superconducting proximity effect and Majorana fermions at the surface of a topological insulator. *Phys. Rev. Lett.* **100**, 096407 (2008).
- [14] Nilsson, J. & Akhmerov, A.R. & Beenakker, C.W.J. Splitting of a Cooper pair by a pair of Majorana bound states. *Phys. Rev. Lett.* **101**, 120403 (2008).
- [15] Tanaka, Y. & Yokoyama, T. & Nagaosa, N. Manipulation of the Majorana fermion, Andreev reflection, and Josephson current on topological insulators. *Phys. Rev. Lett.* **103**, 107002 (2009).
- [16] Hasan, M.Z. & Kane, C.L. Colloquium: topological insulators. *Rev. Mod. Phys.* **82**, 3045-3067 (2010).
- [17] Qu, D.X. & Hor, Y.S. & Xiong, J. & Cava, R.J. & Ong, N.P. Quantum oscillations and Hall anomaly of surface states in the topological insulator  $\text{Bi}_2\text{Te}_3$ . *Science* **329**, 821-824 (2010).
- [18] Xiu, F. *et al.* Manipulating surface states in topological insulator nanoribbons. *Nat. Nano.* **6**, 216-221 (2011).
- [19] Analytis, J.G. *et al.* Two-dimensional surface state in the quantum limit of a topological insulator. *Nat. Phys.* **6** 960-964 (2010).
- [20] Xiong, J. & Petersen, A.C. & Qu, D. & Cava, R.J. & Ong, N.P. Quantum oscillations in a topological

- insulator  $\text{Bi}_2\text{Te}_2\text{Se}_2$  with large bulk resistivity ( $6\Omega\text{cm}$ ). arXiv:1101.1315v1 (2011).
- [21] Taskin, A.A. & Ren, Z. & Sasaki, S. & Segawa, K. & Ando, Y. Observation of Dirac holes and electrons in a topological insulator. *Phys. Rev. Lett* **107**, 016801 (2011).
- [22] Zhang, D. *et al.* Observation of the superconducting proximity effect and possible evidence for Pearl vortices in a candidate topological insulator. *Phys. Rev. B* **84**, 165120 (2011).
- [23] Sacépé, B. *et al.* Gate-tuned normal and superconducting transport at the surface of a topological insulator. *Nature Comm.* **2**, 575 (2011).
- [24] Li, A.H. *et al.* Electronic structure and thermoelectric properties of  $\text{Bi}_2\text{Te}_3$  crystals and graphene-doped  $\text{Bi}_2\text{Te}_3$ . *Thin Sol. Films.* **518** 57-60 (2010).
- [25] Teweldebrhan, D. & Goyal, V. & Rahman, M. & Balandin, A.A. Atomically-thin crystalline films and ribbons of bismuth telluride. *Appl. Phys. Lett.* **96**, 053107 (2010).
- [26] Lifshitz, I.M. & Kosevich, A.M. Theory of magnetic susceptibility in metals at low temperatures. *Sov. Phys. JETP* **2**, 636-645 (1956).
- [27] Brüne, C. *et al.*, Quantum Hall effect from the topological surface states of strained bulk HgTe. *Phys. Rev. Lett.* **106** 126803 (2011).
- [28] Novoselov, K.S. *et al.* Two-dimensional gas of massless Dirac fermions in graphene. *Nature* **438**, 197-200 (2005).
- [29] Zhang, Y. & Tan, Y.W. & Stormer, H.L. & Kim, P. Experimental observation of the quantum Hall effect and Berry's phase in graphene. *Nature* **438**, 201-204 (2005).
- [30] Barzykin, V. & Zagoskin, A.M. Coherent transport and nonlocality in mesoscopic SNS junctions: anomalous magnetic interference patterns. *Superlat. and Microstruct.* **25**, 797-807 (1999).
- [31] Brinkman, A. & Golubov, A.A. Coherence effects in double-barrier Josephson junctions. *Phys. Rev. B* **61**, 11297 (2000).
- [32] Galaktionov, A.V. & Zaikin, A.D. Quantum interference and supercurrent in multiple-barrier proximity structures. *Phys. Rev. B* **65**, 184507 (2002).
- [33] Dietl, T. Dingle temperature in HgSe. *J. Phys. Colloques* **39**, 1081-1083 (1978).
- [34] Gor'kov, L.P. On the energy spectrum of superconductors. *Zh. Eksp. Teor. Fiz.* **34**, 735-739 (1958) [*Sov. Phys. JETP* **7**, 505-508 (1958)].
- [35] Eilenberger, G. Transformation of Gor'kov's equation for type 2 superconductors into transport-like equations. *Z. Phys.* **214**, 195-213 (1968).
- [36] Usadel, K.D. Generalized diffusion equation for superconducting alloys. *Phys. Rev. Lett.* **25**, 507-509

(1970).

- [37] Bergeret, F.S. & Volkov, A.F. & Efetov, K.B. Josephson current in superconductor-ferromagnet structures with a nonhomogenous magnetization. *Phys. Rev. B* **64**, 134506 (2001).
- [38] Zaitsev, A.V. Quasiclassical equations of the theory of superconductivity for contiguous metals and the properties of constricted microcontacts. *Zh. Eksp. Teor. Fiz.* **86**, 1742 (1984) [*Sov. Phys. JETP* **59**, 1015-1024 (1984)]
- [39] Kupriyanov, M.Yu. & Lukichev, V.F. Influence of boundary transparency on the critical current of “dirty” SS’S structures. *Zh. Eksp. Teor. Fiz.* **94**, 139 (1988) [*Sov. Phys. JETP* **67**, 1163-1168 (1988)]
- [40] Blonder, G.E. Tinkham, M. Klapwijk, T.M. Transition from metallic to tunneling regimes in superconducting microconstrictions: Excess current, charge imbalance, and supercurrent conversion. *Phys. Rev. B* **25**, 4515 (1982).

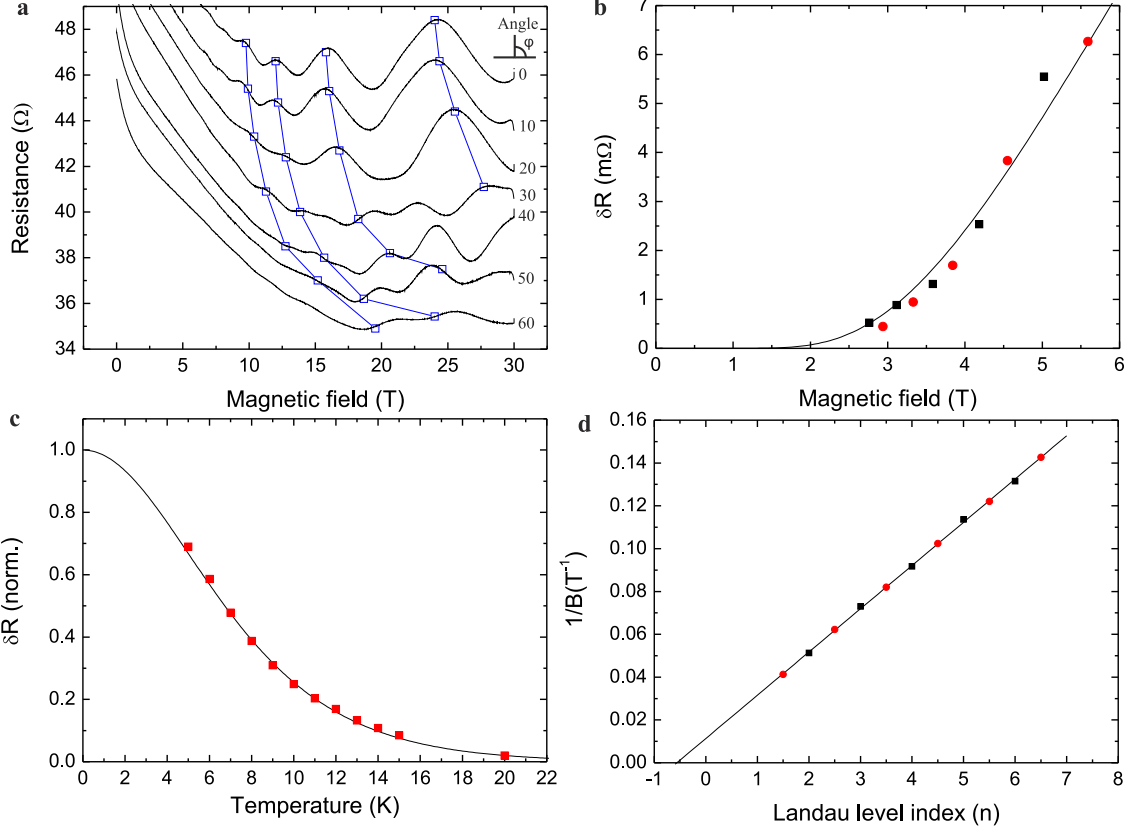


FIG. 2: **Magnetoconductance oscillations of the  $\text{Bi}_2\text{Te}_3$  surface states.** (a) Angle dependence of the Shubnikov-de Haas oscillations, at 4.2 K, (top to bottom: the angle between the magnetic field and the surface normal  $\phi = 0^\circ$  to  $60^\circ$  in steps of  $10^\circ$ ) after linear background subtraction. The square markers represent the expected shift of the maxima in magnetic field for a two dimensional system, given by  $B_\perp = B \cos(\phi)$ , indicating that the oscillations arise from surface states. (b) Oscillation amplitude dependence on the magnetic field (minima as black squares and maxima as red circles); linear backgrounds have been subtracted leaving the oscillating part. We deduce a Dingle temperature  $T_D = 1.65$  K from fitting the increase in oscillation amplitude with increasing field. Only the magnetoconductance in small fields is considered, where the peak splitting is negligible. (c) Oscillation amplitude dependence on temperature; linear backgrounds have been subtracted. The effective mass  $m^* = 0.16 m_0$  is estimated by fitting the decrease of the magnetoconductance oscillations as function of temperature (peaks at least up to 9 T in both the conductance and resistance result in the same effective mass). (d) The  $1/B$  values versus the Landau level index  $n$  intersect at  $n = -0.5$ , consistent with a half filled lowest Landau level as expected for a Dirac cone.

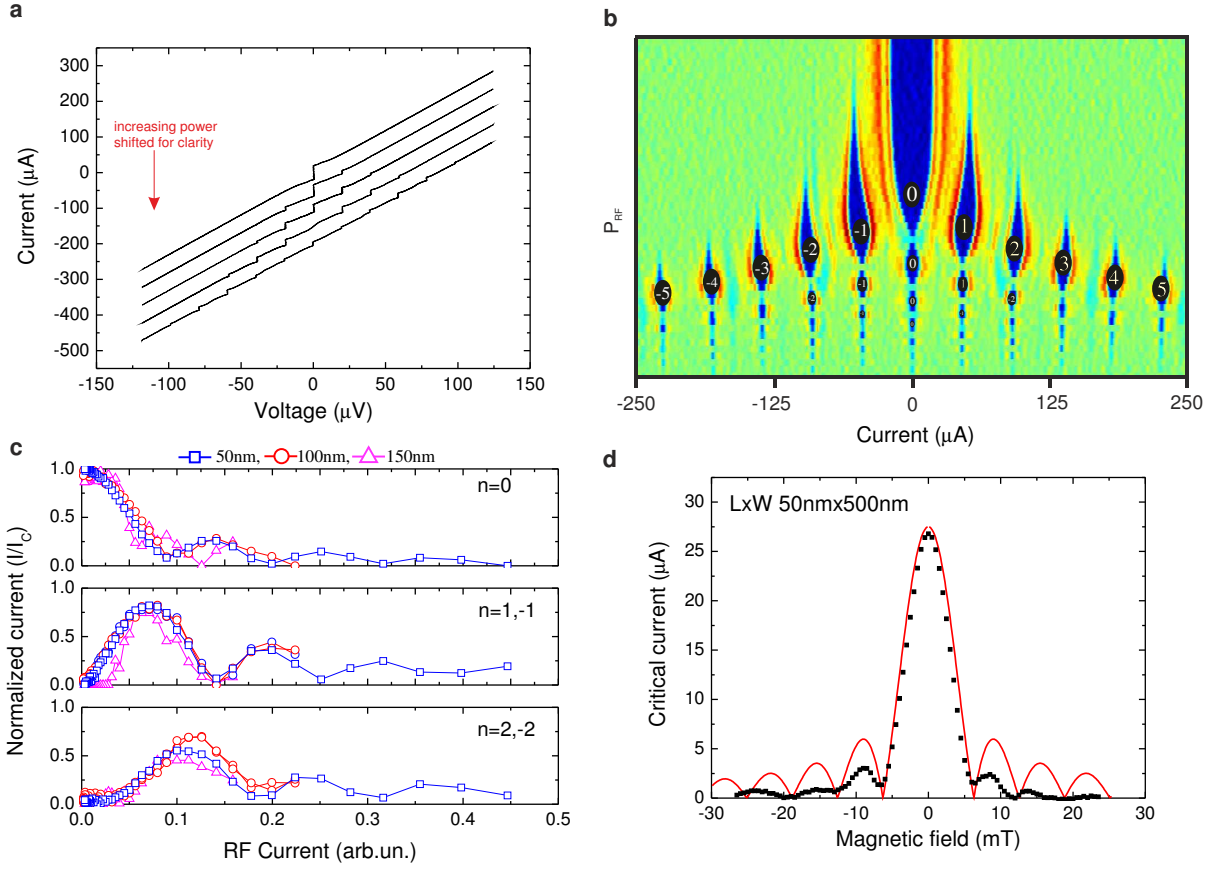


FIG. 3: **Josephson effects.** (a) Current voltage characteristics of a Nb-Bi<sub>2</sub>Te<sub>3</sub>-Nb Josephson junction (length  $l=50$  nm) upon increased 10.0 GHz RF irradiation power (curves are shifted for clarity). The temperature is 1.6 K. Clear Shapiro steps are observed at multiples of  $V = \frac{h}{2e} f_{RF} = 20.7$  μV. (b) Differential resistance,  $dV/dI$ , plotted on a color scale as a function of the bias current,  $I$ , and the microwave excitation power,  $P_{RF}$ . The numbers correspond to the  $n$ -th order Shapiro step. (c) Power dependence of the first three Shapiro steps. Shapiro steps are resolved in the junctions with length up to 150 nm. (d) Critical current dependence on the magnetic field fitted with  $I_C = I_0 \left| \text{sinc} \left( \frac{\pi \Phi}{\Phi_0} \right) \right|$ ,  $I_0$  the critical current at zero field,  $\Phi$  the flux and  $\Phi_0$  the flux quantum. The temperature is 260 mK.

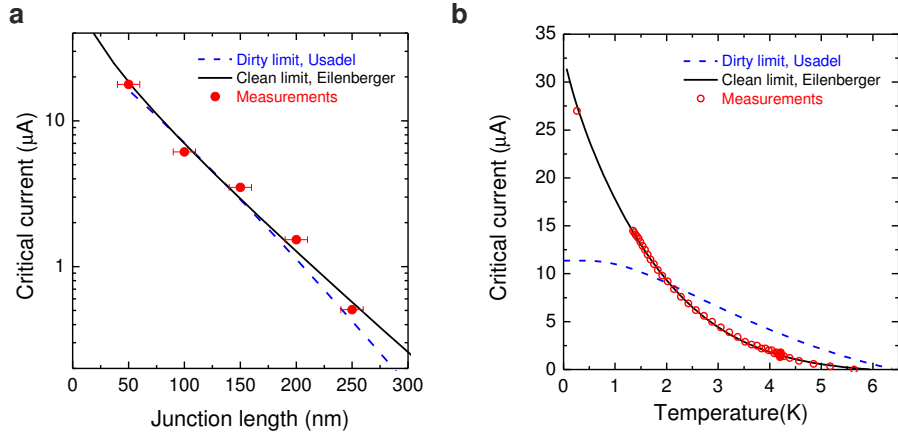


FIG. 4: **Temperature and length dependence of the critical current; demonstration of the ballistic nature of the junctions.** (a) Scaling of the junction critical current with the electrode separation length at 1.6 K. (b) Temperature dependence of the critical current of the 50 nm junction. The measured data (red squares) can only be consistently fitted in both cases with Eilenberger theory for ballistic junctions (dashed black curves), while Usadel theory for diffusive junctions (dotted blue curves) cannot provide a good fit to the temperature dependence of the critical current. See the Supplementary Information for details. The obtained clean limit coherence length  $\xi = 75$  nm at 1.6 K.